Substitutional n-Type Doping of an Organic Semiconductor Investigated by Electron Paramagnetic Resonance Spectroscopy

Si-Guang Chen,[‡] Howard M. Branz,[‡] Sandra S. Eaton,[†] P. Craig Taylor,[§] Russell A. Cormier,[‡,#] and Brian A. Gregg*[,‡]

National Renewable Energy Laboratory, 1617 Cole Boulevard, Golden, Colorado 80401-3393, Department of Chemistry and Biochemistry, University of Denver, Denver, Colorado 80208, Department of Physics, University of Utah, Salt Lake City, Utah 84112-0830, and Department of Chemistry, Metropolitan State College of Denver, Denver, Colorado 80204

Received: January 27, 2004; In Final Form: July 15, 2004

Doping a perylene diimide organic semiconductor with a one-electron reduced perylene diimide containing a covalently bound counterion provides a well-characterized system for understanding doping in organic semiconductors. We obtain insight into the doping process by electron paramagnetic resonance (EPR) measurements of the dopant solutions, the dopant plus host solutions from which thin films are spin-coated, and the resulting solid films. After correction for some trace impurities in the solutions, the spin density incorporated into the solid films is linearly proportional to the added dopant density. Nevertheless, the film conductivity increases superlinearly with dopant concentration. Although neither pure dopant nor host aggregate in solution, they aggregate when combined. This is presumably a result of the delocalization of the dopant electron over a number of host molecules. Angle-dependent EPR measurements on thin films suggest that the **g**-tensor symmetry axis is close to the $\pi-\pi$ stacking axis, consistent with relatively delocalized electrons in this crystal direction. Nevertheless, most electrons are not entirely free, but still bound in the vicinity of the dopant cation by Coulomb attraction. At low concentration, dopants appear to segregate primarily to crystallite grain boundaries, while at higher concentration they are incorporated into the bulk of the crystallites. About half of the spins are paired in the solid at room temperature, and more at lower temperature.

Introduction

The controllable doping of semiconductors was a key enabling advance for the application of inorganic semiconductors such as silicon in modern electronics and optoelectronic devices. Organic semiconductors (OSCs) are now being considered for numerous applications and have already displaced inorganic semiconductors in some low-frequency, large-area applications such as photocopiers and laser printers.[1] Organic light emitting diodes (OLEDs) and flexible organic integrated circuits are on the threshold of becoming commercial products.[2−4] Organic semiconductors may eventually displace their inorganic relatives in many applications that do not need fast switching speeds but require low-cost, large-area, or flexible semiconductors. Our group is investigating the use of doped and undoped organic semiconductors in low-cost photovoltaic solar cells.[5−9]

The doping processes of semiconductors are highly complex and have been the subject of innumerable experimental and theoretical studies.[10,11] Fundamental theoretical aspects of the doping of inorganic semiconductors (ISCs) are still being discussed more than 50 years after the introduction of doped ISCs.[12] Doping of organic semiconductors is just beginning to be quantitatively studied. We present here a study of the doping process in a crystalline, well-characterized OSC.

Doping OSCs is different than doping ISCs. In inorganic semiconductors, the covalent (or covalent-ionic) nature of the interatomic bonds, along with the relatively high dielectric constant and large Bohr radius of charge carriers[13] contribute to the ease of doping. In many ISCs it is actually difficult to produce intrinsic (undoped) materials with a midgap Fermi level. Impurity atoms, distorted or broken bonds at point defects, grain boundaries, and interfaces can all generate unintended electronic states that contribute mobile charge carriers. On the other hand, organic molecular semiconductors are quite difficult to dope. The electronic interactions between the constituent molecules, mainly van der Waals attractions and hydrogen bonds, are quite weak and result in a small Bohr radius of carriers (that is, a localized carrier wave function).[13] Bending or breaking these weak intermolecular bonds does not usually result in electronic gap states that generate mobile electrons or holes. Despite concentrations of chemical impurities and structural defects that are often larger than in ISCs, most OSCs are nearly intrinsic. The weak and unintentional doping observed in most OSCs results primarily from structural defects that tend to preferentially trap electrons (resulting in p-type "doping") or holes (n-type).

A few early studies investigated the effects of purposely added dopants (oxidants or reductants) on the electrical properties of molecular semiconductors.[14−16] Other groups studied the metallic or quasimetallic properties of highly doped molecular compounds.[17−19] Conducting organic polymers were also studied, primarily in their insulating or quasimetallic states.[4,20−23] In some ways, the doped *semiconducting* state of organic materials is more difficult to study than either the intrinsic (insulating) or metallic states. One reason is that the dopants must be bound in the organic lattice to achieve stable semiconducting properties. If the dopants are mobile, p−n junctions

* Address correspondence to this author. E-mail: brian_gregg@nrel.gov.
† University of Denver.
§ University of Utah.
# Metropolitan State College of Denver.
‡ National Renewable Energy Laboratory.

10.1021/jp049628c CCC: $27.50
Published on Web 10/15/2004

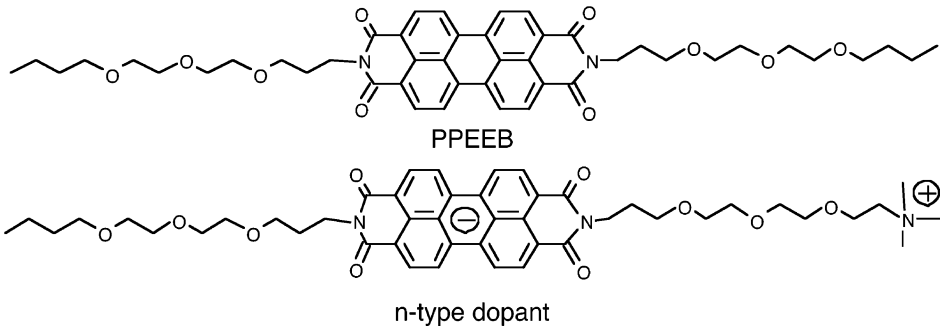

Figure 1. The host semiconductor molecule, PPEEB, and its n-type dopant. When incorporated into the PPEEB lattice, the electron of the dopant is "free" to move along the $\pi-\pi$ stacking axis (perpendicular to the figure plane) while its associated counterion, the quaternized ammonium ion on the side chain, is fixed in the lattice. PPEEB is in its solid phase at room temperature and below.

will disappear with time as the generated charge carriers and their oppositely charged dopant ions diffuse together and recombine.[8,24,25] Because of the weak lattice (intermolecular) forces, it is difficult to dope organic semiconductors with immobile dopants. Most "dopants" employed so far consist of small molecules such as O_2 and Br_2 that diffuse rapidly through the organic film. Some larger molecules such as tetracyanoquinodimethane (TCNQ) have also been used for either surface or bulk doping of organics,[14,15,26−28] and these are expected to diffuse more slowly than the small molecules. Nevertheless, such molecules are incommensurate with the host lattice (that is, they are interstitial rather than substitutional dopants) and have the disadvantage of disrupting crystalline order.

Our approach to studying the doping process in molecular semiconductors[8] is to synthesize a zwitterionic dopant that is a reduced (n-type) analogue of the host molecule (see Figure 1). This substitutional dopant resides in the crystalline host lattice causing minimal structural perturbation and immobilizing the positive counterion. This approach pioneers a doping process for OSCs that places the dopant in well-defined sites, avoids unnecessary complications, and is as similar as possible to the doping of ISCs. Note, however, that along the conducting pathway (the $\pi-\pi$ stacking axis), the dopant is chemically identical with the lattice: it is *not* a chemical defect as are dopants in ordinary inorganic semiconductors. The only "defect" is the positive countercharge that resides in the nonconducting, hydrocarbon-like part of the film.[29]

The conductivity of doped PPEEB films increases superlinearly with dopant concentration as we reported earlier.[8] This superlinear behavior appears to be universal: it is observed in all doped OSCs of which we are aware.[4,19,21−23,26−28,30] Based on some of the results described here, we presented recently a simple model that explains the universality of this behavior.[31] The model considered the strong electrostatic attraction between electrons and dopant cations and the small Bohr radius in OSCs (i.e., the same factors that lead to exciton formation upon light absorption)[9,13] as well as the increase in effective dielectric constant resulting from addition of the highly polarizable dopant molecules, most of which do not produce free electrons.[31] These considerations predict a superlinear increase in free carrier density with increasing doping density for *all* doped OSCs.

In our system, even at 1% doping, most dopant electrons are still bound near a cation at room temperature. The solid-state results we present below are therefore dominated by bound electrons in PPEEB films rather than by the few free electrons. The goal of the present work is to characterize more completely the doping process in organic semiconductors. Because n-type doping introduces π^* antibonding electrons with unpaired spins, our experimental investigations are centered upon electron paramagnetic (or spin) resonance (EPR) characterization of the doped films and the solutions from which they are made.

Experimental Section

The dopant and PPEEB were synthesized as described previously.[7,8,32] Solutions of these two compounds, and PPEEB films with and without dopant, were prepared in a nitrogen atmosphere glovebox. The PPEEB films are doped by adding aliquots of the dopant solution to the solution of PPEEB and then spin-coating onto planar substrates or drying onto EPR tube walls. Solid films of PPEEB undergo a spontaneous transition from a red to a black phase;[7,32] all measurements were performed in the thermodynamically stable black phase. Samples for external measurements were sealed before removal from the glovebox with plastic caps and Parafilm for short-term experiments or with UV-curable epoxy (Norland 121) for longer experiments. Tetrahydrofuran (THF) was purified by refluxing over sodium followed by distillation. Acetonitrile was purified in multiple steps by first refluxing over, and then distilling from (1) $AlCl_3$, (2) $KMnO_4$, (3) $KHSO_4$, and (4) CaH_2. The EPR standards, TEMPO and DPPH, were purchased from Aldrich and used as received. For the EPR experiments, we employed NMR tubes (Pyrex, 4.24 mm i.d.), EPR tubes (quartz, 3.24 mm i.d.), and capillary tubes (Pyrex, 1 mm i.d.); we confirmed that none of these tubes produced an EPR signal by itself.

A Bruker ELEXSYS 5003 X-band (9.8 GHz) EPR spectrometer was employed for EPR measurements. Both the internal Bruker frequency counter and an external Eldorado Model 990 counter were employed for microwave frequency measurements. For solution measurements, 30 μL of solution was placed in a tube and sealed. For solids, 200 μL of the appropriate solution was evaporated in a tube over 1−3 days, which was then sealed and measured. The measurement power, P, was either 0.50 or 0.80 mW; we confirmed by checking the linearity of signal versus $P^{1/2}$ that P was significantly below saturation at all temperatures and dopant concentrations, for both solutions and solids. Also, no saturation effects on line shape were observed. The receiver gain was 30 dB; the 100 kHz amplitude modulation was 1 G to measure spin density and 0.1 or 0.05 G to study line shape. More scans were employed for the low doped samples; sweep time was 20 s. The g-values were calculated relative to a DPPH standard ($g = 2.0036$) with absolute accuracy of ± 0.0002. A Bruker ELEXSYS temperature controller was used to vary the temperature from 310 to 130 K; measurements were made at 10 deg intervals after waiting 10 min for sample equilibration. An HP 8453 spectrometer was employed to measure optical absorbance spectra.

Some measurements were made on a flat film of doped PPEEB. In this case, a solution of 9870 ppm (9.5×10^{18} cm^{-3})

doped PPEEB was spin-coated onto a 0.5 cm × 2 cm microscope slide. After drying and its transition into the black phase, it was sealed with another piece of glass and epoxied around the edges. The EPR signals were measured as a function of the angle between the film normal and the magnetic field.

The quantity of spins (*S*, obtained by double integration of the original signal) was measured for a series of known TEMPO concentrations in THF solution. From this working curve, we calculated the absolute spin densities in both solutions and solids. We estimate that absolute spin densities are accurate to ±40% in solutions but may be accurate to only about a factor of 2 for the solids because of the different sample geometries and microwave absorption which lead to different cavity *Q*. Relative spin densities among samples with identical geometry (i.e., among all films and among all solutions) are accurate to within ±20%. A standard working curve was measured for each sample holder: NMR tubes, EPR tubes, and capillary tubes.

Results and Discussion

Spin-coated films of PPEEB on planar substrates form a highly ordered, smectic C-like phase. Almost independent of deposition conditions or substrates, the undoped films form a characteristic structure consisting of layers of PPEEB with the highly conducting ($\pi-\pi$ stacking) axis parallel to the substrate.[29] The samples are polycrystalline with a 3−10 μm grain size. Polarized light microscopy, X-ray diffraction, and electrical measurements all suggest that the film structure is unperturbed by the presence of the dopant molecules, at least up to our highest dopant concentration of ~1%. The crystals are triclinic; the long axis of the PPEEB molecules is tilted away from the perpendicular to the substrate along both axes orthogonal to the $\pi-\pi$ stacking axis, resulting in π-systems whose normals are tilted at 47° to the substrate. The orientation of the tilt angle is fixed in each crystallite, but random among different crystallites. We have no evidence that evaporating the solutions onto EPR tube walls changes this structure.

Dopants in Solution. One goal of this research was to determine if the superlinear increase in conductivity of the PPEEB films with increasing dopant concentration is a fundamental characteristic of doping organic semiconductors or is related to some unexpected feature of the doping process. We therefore measured EPR spectra in THF solutions of the pure dopant and the dopant plus PPEEB (pure PPEEB solutions showed no EPR signal, as expected). The density of observed spins, *S*, was measured as a function of the density of dopant molecules in solution. There was no observable difference in *S* if PPEEB was included in the solution or not (so we have included both sets of data in Figure 2). This shows that there was no quenching of dopant spins by possible impurities in the PPEEB. The dopant plus PPEEB solutions are the same solutions we employed for spin-coating doped films of PPEEB to measure their conductivity.[8,31] At low concentration, we observed a superlinear increase in *S* with added dopant concentration while *S* became approximately linear at high concentrations (Figure 2). Within our experimental accuracy, each dopant molecule contributes one spin for solution concentrations above about 10^{17} cm^{-3}.

Because this solution behavior could potentially contribute to the superlinear increase in conductivity with increasing dopant concentration, we carefully considered a number of possible mechanisms that might lead to a superlinear increase of *S* with dopant concentration in equilibrium solution. These mechanisms all required some aggregation of the dopant at low concentration leading to spin-paired (EPR silent) species, and production of

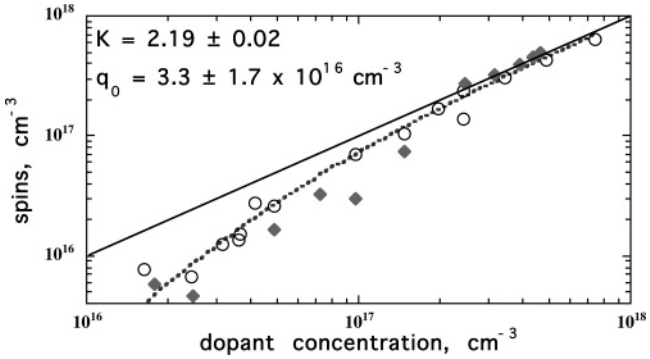

Figure 2. Density of spins in THF solution versus density of dopant molecules. The data include pure dopant solutions (open circles) and dopants in PPEEB solutions (solid diamonds). The spin data are decreased by 30% to account for a calibration error: the spin-to-dopant ratio was set to 1:1 at high dopant concentration. The fit (dashed line) is to eq 3, which assumes there is some trace impurity, *q*, that reversibly removes spins at low dopant concentration. The solid line shows the linear relationship expected if there were no quenching impurities.

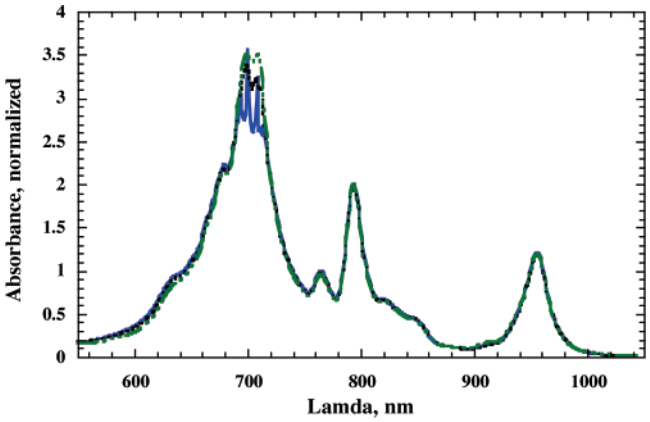

Figure 3. Four normalized absorption spectra of the dopant in THF solution over an 80-fold concentration range, showing no evidence of aggregation.

higher aggregates with observable spin at higher concentrations. We concluded that no equilibrium mechanism involving aggregation of the dopant molecules to produce spin-paired species could be responsible for the observed behavior. Mechanisms involving facile dimerization of dopants (producing spin-paired species) at low concentrations and weak trimerization (producing spin $^1/_2$ species) at higher concentrations could result in a superlinear increase of *S* with dopant concentration over a small concentration range, but only at unphysically high concentrations. We showed that this mechanism cannot be valid in our concentration range: it would result in an average slope, $dS/dn_0 = {}^1/_3$ (n_0 = added dopant concentration), and in $S/n_0 \approx 1/50$. In contrast, we observe $dS/dn_0 \approx 1$ and $S/n_0 \approx 1$ at our highest concentration. In other words, we observe approximately one spin per added dopant molecule at high concentration; it is only at low concentration that spins are "missing".

We also measured the absorption spectra of the dopant species in THF solution as a function of concentration (Figure 3). Absorption spectra of perylene diimides are known to shift substantially upon aggregation of the chromophores.[33,34] Yet solutions of the dopants showed no shifts in absorption spectra with concentration (Figure 3), suggesting again that the dopants do not aggregate in THF solution.

Further confirmation of this important point was provided by EPR spectra of the pure dopant solution run with small magnetic field modulation amplitude. Figure 4 shows the

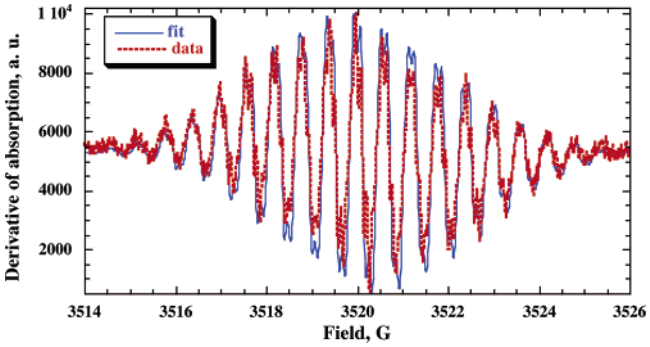

Figure 4. EPR spectrum with 0.05 G modulation of the dopant in acetonitrile solution and simulated fit to these data (see text). The spectrum in THF is similar but with greater solvent broadening (Figure 5). This spectrum strongly suggests that the dopant exists purely as a monomeric species in solution.

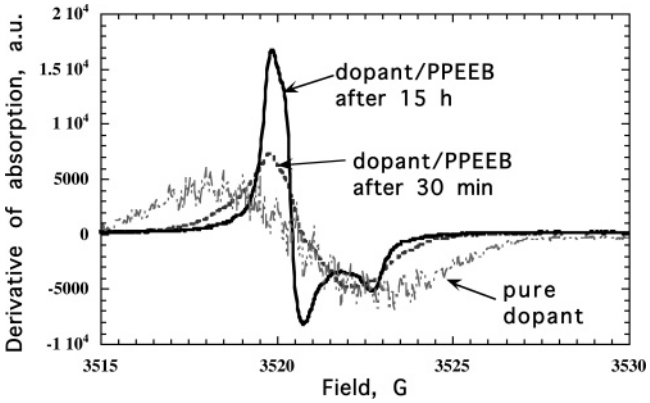

Figure 5. EPR spectra of a 157 μM solution of pure dopant in THF compared to a solution of the same dopant concentration with added PPEEB (120 times dopant concentration). The spectrum evolves from that of a dissolved solution species to that of an aggregate that rotates on a time scale that is slow relative to the microsecond EPR time scale.

experimental EPR spectrum of 188 μM dopant in acetonitrile and a simulation. The agreement is excellent, with hyperfine coupling constants appropriate for a *monomeric* perylene diimide reduced by one electron: 4 H with a hyperfine coupling constant $A = 1.80$ G, 4 H with $A = 0.60$ G, 2 N with $A = 0.57$ G, and a line width of 0.14 G. These parameters account for the substituents on the aromatic rings (Figure 1); there is also a weak coupling we attribute to the first protons on the side chains: 4 H with $A = 0.14$ G. The spectrum is similar to the EPR spectrum reported for naphthalene diimide radical anions.[35] Spectra taken in THF were fit well by the same hyperfine couplings but with greater solvent broadening that resulted in less well-defined peaks (see Figure 5). The EPR line shape of the dopant does not change significantly with concentration in either solvent over the range we measured: 60−190 μM. Moreover, no triplet EPR signal was observed in a thorough search from 1600 to 1900 G.

Taken together, these results and those presented in Figure 5 show that aggregation of dopant molecules in THF solution to dimers and trimers is insignificant. Therefore, aggregation in solution cannot account for the superlinear increase in film conductivity with dopant density. However, the question remains why the spin density of dopants in THF solutions increases faster than linearly at low dopant concentration. The only apparent explanation for this behavior is that some trace impurities in solution *reversibly* quench some of the spins from the dopant. An irreversible quenching model does not fit the data well and it would predict a threshold concentration of dopant below which no EPR signal or conductivity increase would be observed. This does not occur. Although the samples were prepared in a nitrogen atmosphere glovebox in THF distilled from sodium, some oxygen may always be present. The $O_2 \rightarrow O_2^-$ reduction potential[36] is very close to the oxidation potential of the dopant anion,[37] thus reversible quenching is expected. Regardless of mechanism, the actual concentration of dopant present in the PPEEB films was lower than the intended value, especially at low concentration, and this must be taken into account when quantitatively interpreting the data. To quantify the concentration of active dopant in the THF solutions and in the resulting films, we fit the dopant versus spin data (Figure 2) to a simple model assuming the reversible quenching of some fraction of the dopant spins by an unknown quencher, q.

Equilibrium Model for "Missing" Spins in Solution. Let n_0 be the added number of dopants, n_d the effective dopant concentration (the number of observed spins, S, in solution), and n_q the number of quenched spins; then, $n_d + n_q = n_0$. Similarly, let q_0 be the initial number of impurity quenchers, q the equilibrium number of quenchers, and q_r the number of reacted quenchers (which have no observable EPR signal); then, $q + q_r = q_0$. The model is

$$n_d + q \leftrightarrow n_q + q_r \tag{1}$$

and K is the equilibrium constant of the reaction. Expressing the equilibrium in terms of K and eliminating q and q_r leads to

$$K(n_d q_0 - n_d n_0 + n_d^2) = n_0^2 - 2n_d n_0 + n_d^2 \tag{2}$$

This equation can be solved for the number of spins in terms of the added dopant concentration and the initial impurity quencher concentration:

$$n_d = (-Kq_0 - 2n_0 + Kn_0 + K^{1/2}\{Kq_0^2 + 4q_0 n_0 - 2Kq_0 n_0 + Kn_0^2\}^{1/2})/2(K-1) \tag{3}$$

Equation 3 gives an excellent fit to the experimental data (see Figure 2) and provides an equilibrium constant of $K = 2.2$ and a value of $q_0 \approx 3 \times 10^{16}$ molecules/cm^3 in the EPR solution. This value of q_0 should be compared to the values of n_0 ranging from 10^{16} to 10^{18} molecules/cm^3.

The reversible quenching of the dopant's free electron can thus account for the curvature seen in Figure 2. This analysis also provides a means of correcting the added concentration of dopant, n_0, to the concentration actually incorporated into a film, n_d. A working curve based on eq 3 was employed to correct the solution concentrations of n_d. When correcting the values of n_d in solid films, the volume of solution from which a film was obtained (via spin-coating or solvent evaporation into EPR tubes) determines the quencher concentration in the film. The subsequent analyses employ only the corrected values of n_d. This correction amounts to a decrease in effective solution dopant concentration of 50−60% at the lowest concentrations, and is insignificant for the highest concentrations (Figure 2).

Interactions between the Dopant and PPEEB in THF Solutions. We mentioned that the measured number of spins does not change with addition of PPEEB to the dopant solution. However, the EPR spectrum changes substantially, indicating a strong electronic interaction between the dopant and the PPEEB molecules. The EPR spectrum of a pure dopant solution in THF is shown in Figure 5. Also shown are the spectra taken 0.5 and 15 h after addition of PPEEB (which is not EPR active) to the dopant solution in a ratio of 120 PPEEB:1 dopant. Spectra

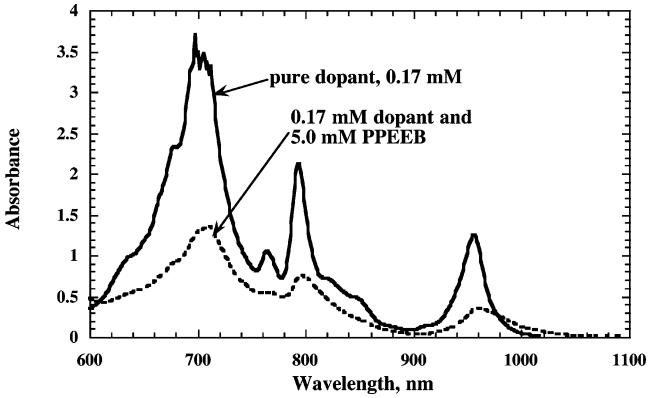

Figure 6. Equilibrium absorption spectra in THF solutions of the pure dopant and of the dopant with PPEEB 20 h after mixing. The dopant concentration is the same in both cases. The PPEEB spectrum is off scale in the region from 400 to 600 nm.

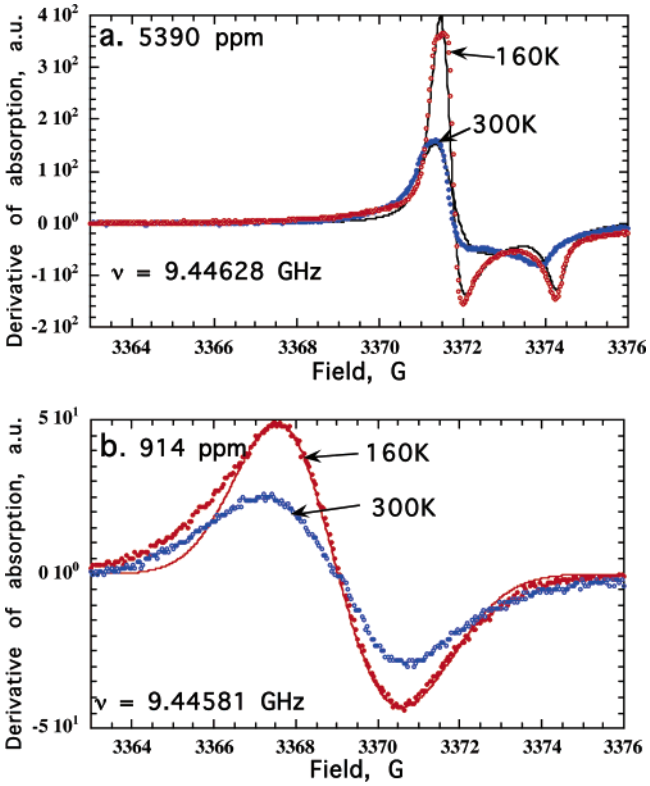

Figure 7. (a) The 5390-ppm doping in solid films at 160 and 300 K and (b) the 914-ppm doping at 160 and 300 K. The solid lines are theoretical fits. Microwave frequencies at 300 K are indicated.

intermediate between these two are observed while the mixture equilibrates. The spectrum evolves from that of a molecularly dissolved solution species showing substantial hyperfine splitting toward that expected for isolated electron spins hopping rapidly among the molecules of a polycrystalline solid (e.g., Figure 7a). The disappearance of the hyperfine splitting after 0.5 h suggests that the electron is averaging many hyperfine environments by hopping on the submicrosecond time scale of the EPR experiment; it is no longer confined to a single chromophore as in the pure dopant solution. The EPR spectrum has already lost reflection symmetry about the line center, indicating an anisotropic **g**-tensor. The subsequent narrowing of the spectrum into a well-defined powder pattern at 15 h confirms the aggregation and shows that the aggregates have become so large that they can no longer rotate on the microsecond time scale. Possibly, there is some precipitation although we see no evidence for it. The aggregates are expected to be approximately 1-dimensional (see below), thus their radius of gyration is very large compared to a spherical species of the same molecular weight. The **g**-tensor giving rise to this powder pattern has elements $g_{zz} = 2.0024$, $g_{xx} = 2.0037$, and $g_{yy} = 2.0040$ where we assign z as the symmetry axis of this **g**-tensor, which is nearly $x-y$ rotationally symmetric. Both the 0.5 and 15 h spectra are fit by the same anisotropic **g**-tensor, but with a broadening that decreases from 2 (0.5 h) to 0.6 G (15 h), presumably as the aggregate size increases and rotation slows.

Neither the dopant nor the PPEEB solutions aggregate by themselves at these concentrations. The driving force for aggregation of the two together is probably the decrease in free energy of the aggregates caused by delocalization of the electron over multiple chromophores. This behavior suggests that spin-coated films of doped PPEEB contain preformed aggregates of one dopant molecule with a number of PPEEB molecules.

To further confirm the aggregation between dopant and PPEEB, absorption spectra of a dopant solution with and without added PPEEB were measured. Only the part of the spectrum showing the dopant absorption is shown in Figure 6 because the PPEEB absorption is off scale. The oscillator strength of the dopant is apparently reduced by about a factor of 3 upon adding PPEEB and equilibrating for 20 h, and the peaks are broadened. This is consistent with aggregation of the dopant with PPEEB molecules and delocalization of the dopant electron over some of the PPEEBs. However, we cannot exclude the possiblity that some precipitation occurrs in these optically dense solutions and contributes to the absorption decrease.

Dopants in Solid PPEEB. EPR spectra at the highest dopant concentrations are powder patterns, as shown in Figure 7a for 5390-ppm films at both 300 and 160 K. The powder pattern is characteristic of electron spins in a spherically symmetric distribution of anistropic local environments.[38] In these polycrystalline PPEEB films, crystallite $\pi-\pi$ stacking axes are expected to be isotropically distributed in the plane of the film. For our films coating a cylindrical tube, therefore, all angles between the $\pi-\pi$ axis and the applied magnetic field are equally probable and a powder pattern is observed. The powder pattern fits to the spectra are shown in Figure 7a. The Lorentzian broadenings are 1.3 and 0.6 G at 300 and 160 K, respectively. Cooling the more heavily doped samples always narrows this angle-independent portion of the line width, probably by reducing the thermal disorder of the molecular solid. The **g**-tensor of the spin at 300 K is nearly axially symmetric about an axis we call z, with $g_{zz} = 2.0021$, $g_{xx} = 2.0034$, and $g_{yy} = 2.0035$. This **g**-tensor is similar to that of the doped aggregates in THF solution reported above; the small differences are likely due to solvent effects. We did not record accurate microwave frequencies at 160 K, so exact g-values cannot be determined. Because g_{zz} is close to the free electron value, however, it should be nearly unchanged at 160 K; with this assumption, $g_{xx} = 2.0036$ and $g_{yy} = 2.0038$ at 160 K. Thus, the 5390-ppm film **g**-tensor becomes slightly less axially symmetric when the temperature is lowered.

In contrast, EPR spectra of low-doped solids of PPEEB are isotropic, with line shapes determined by inhomogeneous (angularly independent) broadening. The 914 ppm film spectrum at 160 K is shown with our best fit to the data in Figure 7b. The spectrum is Gaussian broadened by 3.0 G from the identical solid film **g**-tensor as found in the 5390-ppm film. The broadening destroys the resolved features of the EPR powder pattern. The large inhomogeneous broadening of the low-doping line suggests a distribution of environments for the spins. One

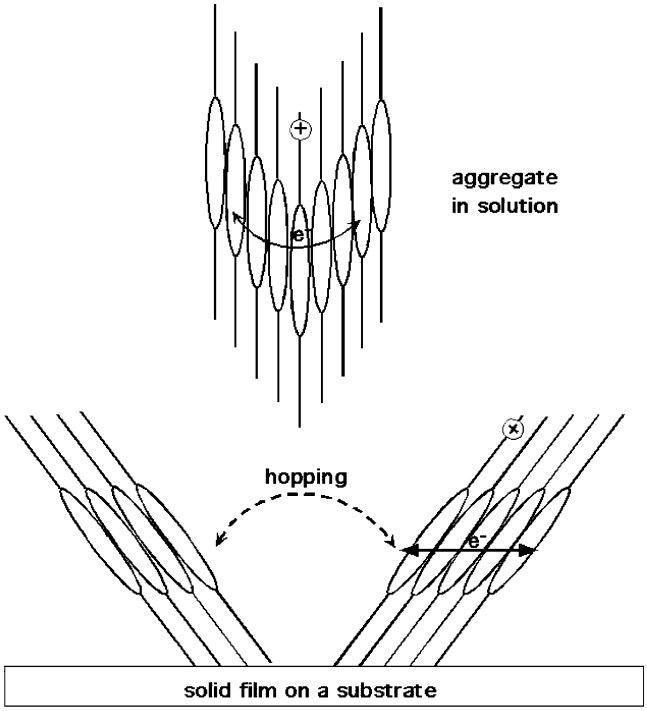

Figure 8. Proposed structure of aggregates formed in solution that leads to incorporation of dopants at grain boundaries. The lower figure is a 1-D representation of a 2-D film; it thus exaggerates the average spacing between crystallites.

interpretation of the broadening is that at low concentration, dopants segregate primarily to disordered grain boundaries between the crystallites (see Figure 8 and discussion below). At higher dopant concentrations, dopants are found primarily inside the crystallites, where neighboring molecules share the same orientation and the ensemble of bulk electrons exhibit the polycrystalline powder pattern. Improved fits to the 300 K, 5390-ppm spectrum, compared to what is shown in Figure 7a, can be obtained by adding a 3.0 G broadened isotropic line to the powder pattern, with an intensity ratio of about 1:3. This probably indicates that some grain boundary spins are also present in the highly doped films.

The hypothesis of spins at the grain boundaries is consistent with the known crystal structure. PPEEB molecules form a specific low-energy structure with a longitudinal offset between chromophores of ~3.1 Å, a transverse offset of ~0.8 Å, and a $\pi-\pi$ stacking distance of ~3.4 Å.[29] If we assume that the dopant aggregates with PPEEB in THF solution have a similar structure, the lowest energy aggregate in solution would be "V-shaped" since this brings the partially delocalized electron on the chromophores closest to the positive charge on the side chain of the dopant (Figure 8).

However, this V-shaped aggregate is not compatible with the structure of solid films:[29] one-half of the "V" would have to rotate to a different orientation to form the smectic-C-like phase of the solid films, as shown schematically in Figure 8. This would leave a dopant molecule at the grain boundary between the two crystallites. Not shown in Figure 8 is the relatively disordered structure at the grain boundary. Since the crystallite size is observed to be independent of doping density, so also must be the area available to grain boundaries. At high doping concentration, therefore, some of the dopants will be incorporated inside the crystallites.

The EPR spectra of a 9870 ppm doped film (Figure 9) deposited on flat glass are anisotropic powder patterns when the substrate normal is oriented at 45, 60, or 90° to the applied

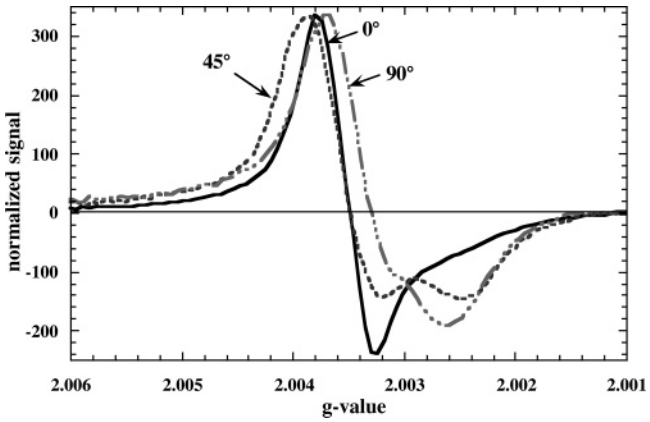

Figure 9. The normalized EPR spectra of a thin film of doped PPEEB on glass as a function of the angle between the substrate normal and the magnetic field, *H*. At 0° the two are collinear; at 90° they are perpendicular.

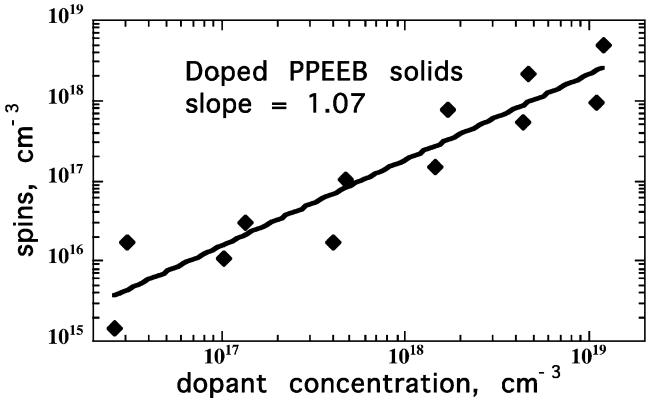

Figure 10. A plot of spin density versus dopant concentration, n_d, for doped PPEEB solids. The solid line is a power law fit to the data.

magnetic field (*H*) and a nearly isotropic line only at 0°, i.e., with the substrate normal parallel to *H*. The isotropic spectrum at 0° is caused by the fixed tilt angle relative to the substrate assumed by all molecules (see Figure 8; the *orientation* of the tilt angle in different crystallites, however, is random): both chromophore rings and $\pi-\pi$ stacks make a unique angle (47° and 90°, respectively) with the substrate normal in every crystallite.[29]

The observed 0° *g*-value of $g_0 = 2.0035$ is comparable to g_{xx} and g_{yy} derived from the full axially symmetric powder pattern, but is very different from the principal axis component $g_{zz} = 2.0021$. The lack of significant admixture of g_{zz} into g_0 suggests that the principal symmetry axis of the spin **g**-tensor is nearly parallel to the substrate; that is, the *z*-axis is nearly parallel to the $\pi-\pi$ stacking axis. We would expect this symmetry if the electron is delocalized among many perylene diimide molecules. However, the symmetry could be broken by the ring symmetry (principal axis tilted 47° toward the substrate normal) and the electrostatic attraction to the ionic charge.

The density of spins as a function of dopant concentration was measured in the solid PPEEB samples. After correction for the quencher concentration, the spin density in the films increases linearly with dopant concentration as shown in Figure 10. In other words, the film spin density is proportional to the spin density in the solution from which it is spun. However, $S \approx 0.3n_d$, suggesting that some spin-pairing occurs in the solid, see below. As mentioned earlier, calibration errors introduced by differences between solution and film samples introduce a factor of ~2 uncertainty in *S*.

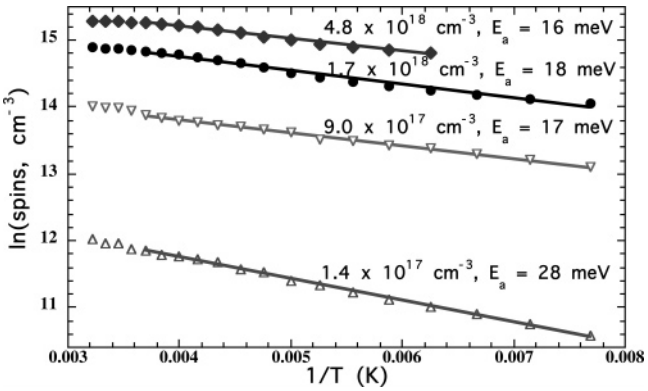

Figure 11. The temperature dependence of the spin density of solid films displayed on an Arrhenius plot for different doping concentrations. The measured spin signal is divided by *T* to obtain the Curie-corrected spin densities.

Temperature (*T*)-dependent studies of the spin density in solid films of different dopant concentration are shown in Figure 11. The abscissa displays the spin density after the Curie correction for the temperature dependence of spin statistics. The reversible decrease in spin density with decreasing temperature suggests that spin pairing is occurring in the doped films. At the highest dopant concentration shown, 0.58% (4.8×10^{18} cm^{-3}), the spin density decreases at low *T* with an apparent activation energy of $E_a = 16$ meV, and begins to saturate near room temperature where kT exceeds E_a. At the lowest concentration measured, 1.4×10^{17} cm^{-3}, the activation energy increases to 28 meV.

Spin pairing in the solid films would place two dopant electrons in the same electronic orbital. This orbital may be near a single cation (which has no spin), leaving the second "bare", or it may be between two cations. In either case, the free energy of spin-pairing must overcome the electrostatic repulsions between the two electrons and the two cations. From our data, spin-pairing is slightly favored at room temperature, becoming more favored at low doping density and low temperature. This may be an entropy-driven effect, considering that dopant electrons become more delocalized (less tightly bound) at higher doping densities[31] and higher temperatures, and are thus less likely to form localized spin-pairs. It may also be affected by the dopant's tendency to segregate to grain boundaries at low dopant concentration. At room temperature, the degree of spin pairing ranges from ~70% at low doping concentration to ~50% at high concentration. This is probably responsible for the fact that $S < n_d$ in Figure 10. We do not yet know if spin-pairing also influences the conductivity, but given the low activation energy, any effect is expected to be small at room temperature.

Summary and Conclusions

We employed EPR and optical spectroscopy to characterize the doping process in a liquid crystal perylene diimide, PPEEB. Studies of the dopant solutions showed that a small fraction of the dopant is reversibly quenched by an unknown impurity, probably O_2. This led to a model that allowed us to correct for the influence of this impurity. The dopant exists in monomeric form in THF solution, but with the addition of PPEEB it forms aggregates so large that they cannot rotate on the microsecond time scale of the EPR experiments. The driving force for formation of these soluble aggregates is presumably the decrease in free energy caused by delocalization of the dopant electron over a number of host molecules. The **g**-tensor of these solution aggregates is nearly axially symmetric and close to that observed in solid films. Most dopant electrons are delocalized over a number of molecules; angle-dependent measurements in films show that the delocalization is sufficient to approximately align the g-tensor symmetry axis with the $\pi-\pi$ stacking direction. Rapid hopping of these delocalized electrons narrows the EPR line width.

At low dopant concentration and high temperature in solid films, the EPR signal is isotropic with a line width indicating that the spin primarily resides in a disordered environment at crystal grain boundaries. This interpretation is also supported by consideration of the likely structure of dopant/host aggregates in the spin-coating solutions. At higher concentration, dopants also appear in the bulk of the crystals where the more perfect crystal lattice leads to an anisotropic powder pattern spectrum. As temperature is lowered the spectrum of highly doped solid films becomes more anisotropic. Temperature-dependent studies suggest that there is substantial spin-pairing of the dopant electrons, especially at low dopant concentration and low temperature.

Doping PPEEB with an n-type substitutional dopant provides one of the simplest and best characterized systems for doping organic semiconductors. Still, there are numerous complexities in this seemingly simple process. We showed earlier that the strong electrostatic attractions and the relatively localized wave functions of charge carriers control the photophysical properties of OSCs as well as their doping processes.[31] For these reasons, even at our highest doping density, only ~1% of the dopants contribute free electrons at room temperature: thus, the EPR signals derive almost entirely from the *bound* electrons. We are not yet able to characterize the conducting electrons in this low-dimensional conductor except by conductivity measurements. The data obtained here by EPR and optical measurements, along with structural and electrostatic potential data from previous work,[8,29,31] provide a more complete characterization of the doping process in this organic semiconductor.

Acknowledgment. We are grateful to Mark Davis of NREL for helpful discussions and advice. S.C., H.M., and B.G. thank the U.S. DOE, Office of Science, Division of Basic Energy Sciences, Chemical Sciences Division, and also the U.S. DOE Photovoltaic Program under Contract No. DE-AC-36-99GO10337 for supporting this research. P.C.T. thanks the NSF, grant number DMR-0307594, for support.

References and Notes

(1) Law, K.-Y. *Chem. Rev.* **1993**, *93*, 449.
(2) Forrest, S. R. *Chem. Rev.* **1997**, *97*, 1793.
(3) Blom, P. W. M.; Vissenberg, M. C. J. M. *Mater. Sci. Eng.* **2000**, *27*, 53.
(4) Heeger, A. J. *J. Phys. Chem. B* **2001**, *105*, 8475.
(5) Gregg, B. A. *Chem. Phys. Lett.* **1996**, *258*, 376.
(6) Breeze, A. J.; Salomon, A.; Ginley, D. S.; Gregg, B. A.; Tillmann, H.; Hörhold, H.-H. *Appl. Phys. Lett.* **2002**, *81*, 3085.
(7) Cormier, R. A.; Gregg, B. A. *J. Phys. Chem.* **1997**, *101*, 11004.
(8) Gregg, B. A.; Cormier, R. A. *J. Am. Chem. Soc.* **2001**, *123*, 7959.
(9) Gregg, B. A. *J. Phys. Chem. B* **2003**, *107*, 4688.
(10) Debye, P. P.; Conwell, E. M. *Phys. Rev.* **1954**, *93*, 693.
(11) Pearson, G. L.; Bardeen, J. *Phys. Rev.* **1949**, *75*, 865.
(12) Zunger, A. *Appl. Phys. Lett.* **2003**, *83*, 57.
(13) Gregg, B. A.; Hanna, M. C. *J. Appl. Phys.* **2003**, *93*, 3605.
(14) Kearns, D. R.; Tollin, G.; Calvin, M. *J. Chem. Phys.* **1960**, *32*, 1020.
(15) Leempoel, P.; Fan, F.-R. F.; Bard, A. J. *J. Phys. Chem.* **1983**, *87*, 2948.
(16) Loutfy, R. O.; Sharp, J. H. *J. Chem. Phys.* **1979**, *71*, 1211.
(17) Peterson, J. L.; Schramm, C. S.; Stojakovic, D. R.; Hoffman, B. M.; Marks, T. J. *J. Am. Chem. Soc.* **1977**, *99*, 286.
(18) Marks, T. J. *Science* **1985**, *227*, 881.
(19) Almeida, M.; Kanatzidis, M. G.; Tonge, L. M.; Marks, T. J.; Marcy, H. O.; McCarthy, W. J.; Kannewurf, C. R. *Solid State Commun.* **1987**, *63*, 457.

(20) deLeeuw, D. M. *Synth. Met.* **1993**, *57*, 3597.
(21) Reedijk, J. A.; Martens, H. C. F.; Brom, H. B.; Michels, M. A. J. *Phys. Rev. Lett.* **1999**, *83*, 3904.
(22) Jarrett, C. P.; Friend, R. H.; Brown, A. R.; de Leeuw, D. M. *J. Appl. Phys.* **1995**, *77*, 6289.
(23) Zuo, F.; Angelopoulos, M.; MacDiaramid, A. G.; Epstein, A. J. *Phys. Rev. B* **1989**, *39*, 3570.
(24) Guillemoles, J. F.; Lubomirsky, I.; Riess, I.; Cahen, D. *J. Phys. Chem.* **1995**, *99*, 14486.
(25) Lonergan, M. C.; Cheng, C. H.; Langsdorf, B. L.; Zhou, X. *J. Am. Chem. Soc.* **2002**, *124*, 690.
(26) Maennig, B.; Pfeiffer, M.; Nollau, A.; Zhou, X.; Leo, K.; Simon, P. *Phys. Rev. B* **2001**, *64*, 195208.
(27) Pfeiffer, M.; Beyer, A.; Fritz, T.; Leo, K. *Appl. Phys. Lett.* **1998**, *73*, 3202.
(28) Pfeiffer, M.; Beyer, A.; Plönnigs, B.; Nollau, A.; Fritz, T.; Leo, K.; Schlettwein, D.; Hiller, S.; Wörhle, D. *Sol. Energy Mater. Sol. Cells* **2000**, *63*, 83.
(29) Liu, S.-G.; Sui, G.; Cormier, R. A.; Leblanc, R. M.; Gregg, B. A. *J. Phys. Chem.* **2002**, *106*, 1307.
(30) Shen, Y.; Diest, K.; Wong, M. H.; Hsieh, B. R.; Dunlap, D. H.; Malliaras, G. G. *Phys. Rev. B* **2003**, *68*, 081204.
(31) Gregg, B. A.; Chen, S.-G.; Branz, H. M. *Appl. Phys. Lett.* **2004**, *84*, 1707.
(32) Cormier, R. A.; Gregg, B. A. *Chem. Mater.* **1998**, *10*, 1309.
(33) Ferrere, S.; Zaban, A.; Gregg, B. A. *J. Phys. Chem. B* **1997**, *101*, 4490.
(34) Ferrere, S.; Gregg, B. A. *J. Phys. Chem. B* **2001**, *105*, 7602.
(35) Zhong, C. J.; Kwan, W. S. V.; Miller, L. L. *Chem. Mater.* **1992**, *4*, 1423.
(36) Bard, A. J.; Faulkner, L. R. *Electrochemical Methods*; Wiley & Sons: New York, 1980.
(37) Gregg, B. A.; Cormier, R. A. *J. Phys. Chem.* **1998**, *102*, 9952.
(38) Taylor, P. C.; Baugher, J. F.; Kriz, H. M. *Chem. Rev.* **1975**, *75*, 203.